Dalton Transactions

In situ synthesis and high adsorption performance of MoO2/Mo4O11 and MoO2/MoS2 composite nanorods by reduction of MoO3

Journal:	*Dalton Transactions*
Manuscript ID:	DT-ART-10-2014-003067.R2
Article Type:	Paper
Date Submitted by the Author:	16-Feb-2015

Complete List of Authors:	Xu, Bingyu; Key Laboratory of Functional Inorganic Material Chemistry, Ministry of Education of the People's Republic of China, Li, Ying; Key Laboratory of Functional Inorganic Material Chemistry, Ministry of Education of the People's Republic of China, Zhao, Dongdong; Heilongjiang University, Pan, Kai; Key Laboratory of Functional Inorganic Material Chemistry, Ministry of Education of the People's Republic of China, ; Heilongjiang University, School of Chemistry and Materials Science Jiang, Baojiang; Key Laboratory of Functional Inorganic Material Chemistry, Ministry of Education of the People's Republic of China, zhou, wei; Key Laboratory of Functional Inorganic Material Chemistry, Ministry of Education of the People's Republic of China, ; Heilongjiang University, Guofeng, Wang; Heilongjiang University, Fu, honggang; Heilongjiang University,

In situ synthesis and high adsorption performance of MoO_2/Mo_4O_{11} and MoO_2/MoS_2 composite nanorods by reduction of MoO_3

Bingyu Xu, Ying Li, Guofeng Wang*, Dongdong Zhao, Kai Pan, Baojiang Jiang, Wei Zhou, and Honggang Fu*

Key Laboratory of Functional Inorganic Material Chemistry, Ministry of Education, School of Chemistry and Materials Science, Heilongjiang University, Harbin, 150080, China. E-mail: wanggf_w@163.com; fuhg@vip.sina.com

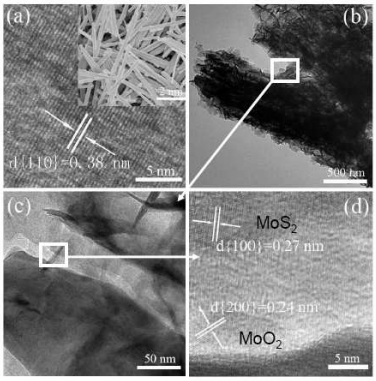

MoO_2/Mo_4O_{11} and MoO_2/MoS_2 composite nanorods with high adsorption performance were successfully synthesized by reducing MoO_3 nanorods.

In situ synthesis and high adsorption performance of MoO_2/Mo_4O_{11} and MoO_2/MoS_2 composite nanorods by reduction of MoO_3

Bingyu Xu, Ying Li, Guofeng Wang*, Dongdong Zhao, Kai Pan, Baojiang Jiang, Wei Zhou, and Honggang Fu*

Received (in XXX, XXX) Xth XXXXXXXXX 200X, Accepted Xth XXXXXXXXX 200X
First published on the web Xth XXXXXXXXX 200X
DOI: 10.1039/b000000x

MoO_2/Mo_4O_{11} and MoO_2/MoS_2 composite nanorods were successfully synthesized by reducing MoO_3 nanorods. The adsorption performance of samples was evaluated by using Rhodamine B (RhB) and metal ions in aqueous solutions as the targets. The results indicated that the obtained MoO_2/Mo_4O_{11} and MoO_2/MoS_2 composite nanorods can present excellent adsorption performance. The BET surface areas of samples increased with increasing the MoO_3:S mass ratio. The adsorption kinetics for the RhB and Cu^{2+} ions on the composite nanorods were well fitted to a pseudo-second order model.

1. Introduction

Chemical, physical, and materials studies on the nanometer scale have experienced an enormous development because the reduction of particle size in crystalline systems can result in remarkable modifications of some of their bulk properties because of a high surface-to-volume ratio and the quantum confinement effect.[1-5] The synthesis of inorganic nanocrystals with controlled shape, size, composition, internal structure, and surface chemistry is of fundamental and technological interest for mapping their shape/size-dependent material properties and for consolidating their promising applications in optics, catalysis, biosensing, and data storage.[6-10] Up to now, various techniques have been developed to synthesize desired nanostructures, such as hydrotherm, microemulsion, sol–gel, and combustion.[11]

With the development of industry and technology, increasing environmental pollution is of major concern, especially water pollution caused by metal ions and dye.[12-14] Heavy metal and dye contamination exists in aqueous waste streams of many industries, which are not biodegradable and tend to accumulate in living organisms causing diseases and disorders. And thus, it is necessary to remove them from contaminated waters. It is well known that the noble metals are widely applied in catalysis processes, electronics, and the chemical industry. However, the noble metals have low natural concentration and high prices.[15,16]

Adsorption is one of the effective and economical ways to separate metal ions and dye from wastewater. Some materials can be used for adsorption applications, such as zeolites, biomaterials, Al_2O_3, carbonaceous materials, and ions exchange resins.[17-20] However, as sorbents, MoO_2/Mo_4O_{11} and MoO_2/MoS_2 composite nanomaterials have never been reported.

Composite materials formed by combining two or more materials could present complementary properties that have shown important technological applications.[3,21] Herein, we successfully prepared MoO_2/Mo_4O_{11} and MoO_2/MoS_2 composite nanorods by reducing MoO_3 nanorods for the first time. The obtained MoO_2/Mo_4O_{11} and MoO_2/MoS_2 composite nanorods can present excellent adsorption performance. The adsorption kinetics for the Cu^{2+} ions and RhB on the composite nanorods were investigated.

2. Experimental section

Analytical grade Na_2MoO_4, $H(NO_3)_3$, and sulphur powder were obtained from Beijing Chemical Co. Ltd. All chemicals were directly used without further purification. For the synthesis of MoO_3 nanorods: Na_2MoO_4 (5 mmol) was dissolved in distilled water (25 mL), and the pH was adjusted to 1 using a dilute HNO_3 solution. The solution was agitated for 30 min. Then it was poured into a stainless steel autoclave with a Teflon-liner of 50 mL capability and heated at 180 °C for 24 h. After cooling to room temperature, the products were collected by means of centrifugation, washed with distilled water, and dried in vacuum at 80 °C. In the synthesis of MoO_2/Mo_4O_{11} and MoO_2/MoS_2 composite nanorods, the as-prepared MoO_3 nanorods and some sulphur powder were put into a crucible, and annealed at 650 °C for 15 min in N_2 atmosphere.

Characterization: The size and morphology of the MoO_3, MoO_2/Mo_4O_{11}, and MoO_2/MoS_2 composite nanorods were characterized with transmission electron microscopy (TEM, JEM 2010 with operating voltage of 200KV) and scanning electron microscopy (SEM, Hitachi S-4800 with operating voltage of 15 kV). Raman spectra of the samples were taken by using a Renishaw 1000 Micro-Raman spectrometer. X-ray photoelectron spectroscopy (XPS) analysis was performed on a VG ESCALABMK II with a Mg KR (1253.6 eV) achromatic X-ray source. Fourier transform infrared spectra of the samples were recorded at room temperature with a Perkin-Elmer Spectrum one FTIR spectrometer using the KBr pellet method.

Dye adsorption experiment: 50 mg of the MoO_2/Mo_4O_{11}, and MoO_2/MoS_2 composite nanorods was added into 50 mL of 5 mgL^{-1} of Rhodamine B (RhB) aqueous solution followed by stirring at room temperature in dark for 5, 10, 15, 20, 25, 30, 35, 40, 45, and 50 min, respectively. The MoO_2/Mo_4O_{11} and

Key Laboratory of Functional Inorganic Material Chemistry, Ministry of Education, School of Chemistry and Materials Science, Heilongjiang University, Harbin, 150080, China. E-mail: wanggf_w@163.com; fuhg@vip.sina.com

MoO_2/MoS_2 composite nanorods with adsorbed RhB were removed by means of centrifugation. The concentration of the solutions was measured with a model UV-5220 UV-Vis spectrophotometer in matched quartz cells, and calculated by the standard spectrophotometric methods at λ=553 nm for RhB. Metal ion adsorption experiment: 50 mg of sample was dispersed in 50 mL of metal salt (500 mg) solution by stirring at room temperature.

Kinetic studies: The first-order rate equation is given as:

$$\log(q_e - q_t) = \log q_e - \frac{k_1}{2.303}t \quad (1)$$

The pseudo-second-order equation is given as:

$$\frac{t}{q_t} = \frac{1}{k_2 q_e^2} + \frac{t}{q_e} \quad (2)$$

Where q_e and q_t are the dye amounts adsorbed on the adsorbents (mg g^{-1}) at equilibrium and at time t, respectively; k_1 and k_2 are the rate constants of first and second order adsorptions, in min^{-1} and g mg^{-1}. In fact, it is required that calculated equilibrium adsorption capacity values, q_e (cal.), should be in accordance with the experimental q_e (exp.) values.

3. Results and Discussion

3.1 Crystal structures and morphologies of samples

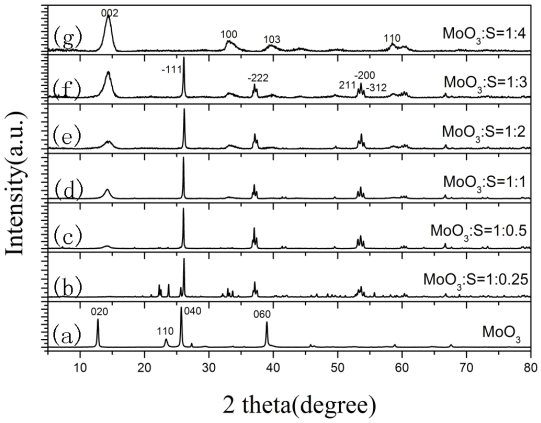

Figure 1. XRD patterns of MoO_2/Mo_4O_{11} and MoO_2/MoS_2 composite nanorods with different MoO_3:S mass ratios.

Table 1. Effect of the MoO_3:S mass ratios on the compositions of samples.

MoO_3:S mass ratios	Compositions of samples
1:0	MoO_3
1:0.25	MoO_2 and Mo_4O_{11}
1:0.5	MoO_2 and MoS_2
1:1	MoO_2 and MoS_2
1:2	MoO_2 and MoS_2
1:3	MoO_2 and MoS_2
1:4	MoS_2

Figure 1(a) shows the XRD pattern of the prepared MoO_3 nanorods. All the diffraction peaks can be indexed to the pure orthorhombic phase MoO_3 (JCPDS 05-0508). No other impurity peaks were detected. Figure 1(b-g) shows the XRD patterns of the composite nanorods with different MoO_3:S mass ratios. When the MoO_3:S mass ratio was 1:0.25, monoclinic phase MoO_2 (JCPDS 32-0671) and orthorhombic phase Mo_4O_{11} (JCPDS 05-0337) were obtained. With increasing the content of sulfur powder, MoO_2 and hexagonal phase MoS_2 (JCPDS 37-1492) were obtained. When the MoO_3:S mass ratio was 1:4, pure MoS_2 were synthesized. The effect of the MoO_3:S mass ratios on the compositions of samples was summed up in Table 1.

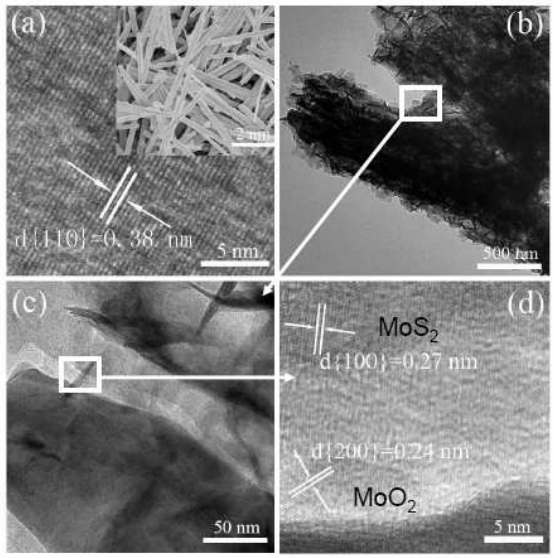

Figure 2. (a) SEM (inset) and HRTEM images of MoO_3 nanorods. (b-d) HRTEM images of MoO_2/MoS_2 (MoO_3:S=1:3) composite nanorods.

The corresponding scanning electron microscope (SEM) and high-resolution transmission electron microscope (HRTEM) images of MoO_3 nanorods are shown in Figure 2(a). The MoO_3 nanorods are ~ 200 nm in diameter and ~ 4 μm in length. Typical HRTEM image of a single nanorod shows an interplanar spacing of 0.38 nm corresponding to the ⟨110⟩ plane of orthorhombic phase MoO_3. Figure 2(b-d) shows the TEM and HRTEM images of the MoO_2/MoS_2 (MoO_3:S=1:3) composite nanorods. The HRTEM image of a single composite nanorod shows interplanar spacings of 0.24 and 0.27 nm corresponding to the ⟨200⟩ plane of MoO_2 and ⟨100⟩ plane of MoS_2, respectively.

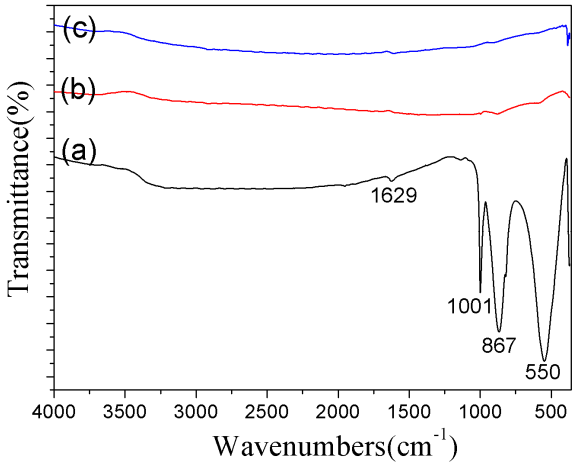

Figure 3. FTIR spectra of (a) MoO_3, (b) MoO_2/MoS_2 (MoO_3:S=1:2), and (c) MoO_2/MoS_2 (MoO_3:S=1:4).

In addition, the surfactant overlayer of the nanorods was identified with Fourier transform infrared (FTIR) studies, as shown in Figure 3. For MoO_3 nanorods, the band at 1629, 1001,

and 867, 550 cm^{-1} are attributed to the characterizing modes of nitrate. However, for MoO_2/MoS_2 composite nanorods, the characterizing modes of nitrate vanished due to the high-temperature treatment during the vulcanization process.

Figure 4 shows the XPS spectra of MoO_2/MoS_2 (MoO_3:S=1:3) composite nanorods. Obviously, Mo^{4+} has been identified by its Mo 3P and Mo 3d peaks, O^{2-} has been identified by O 1s peak, and S^{2-} has been identified by S 2p peaks. On the low binding energy side of the Mo 3d components is detected the S 2s peak at 226.5 eV. In addition, the S 2p spectrum can be fitted by four peaks located at 161.8, 162.2, 162.9, and 163.1 eV, as shown in Figure 4(d).

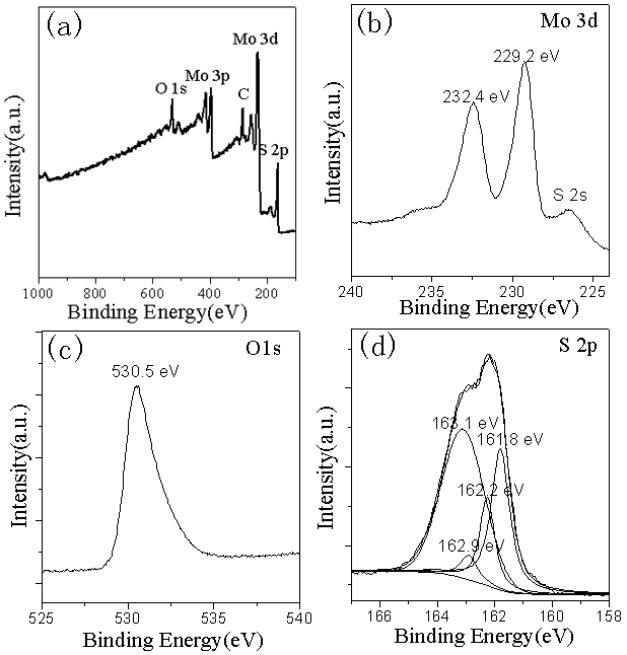

Figure 4. (a) The survey XPS spectrum of MoO_2/MoS_2 (MoO_3:S=1:2) composite nanorods. (b-d)) XPS Mo 3d, O 1s, and S 2p spectra of MoO_2/MoS_2 (MoO_3:S=1:2) composite nanorods.

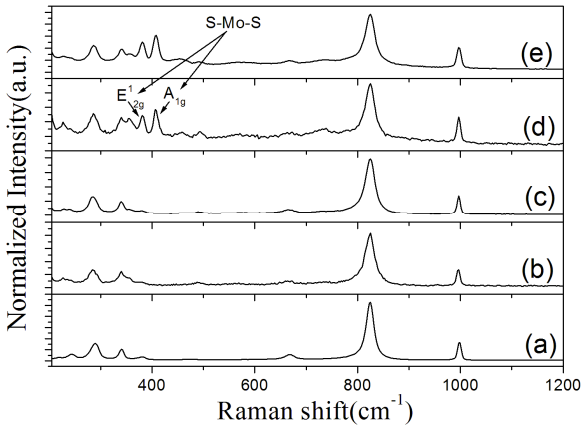

Figure 5. Raman spectra of (a) MoO_3, (b) MoO_2/Mo_4O_{11} (MoO_3:S=1:0.25), (c) MoO_2/MoS_2 (MoO_3:S=1:0.5), (d) MoO_2/MoS_2 (MoO_3:S=1:1), and (e) MoO_2/MoS_2 (MoO_3:S=1:2).

Figure 5 shows the Raman spectra of MoO_2/MoS_2 (MoO_3:S=1:2) composite nanorods. The Raman peaks of MoS_2 appear at 383 and 408 cm^{-1}, which can be attributed to the E^1_{2g} and the A_{1g} vibrational modes from S-Mo-S, respectively.

3.2 adsorption performance of MoO_2/Mo_4O_{11} and MoO_2/MoS_2 composite nanorods

The performance of MoO_2/Mo_4O_{11} and MoO_2/MoS_2 composite nanorods was evaluated by the adsorption performance of RhB in aqueous solution under dark condition. Figure 6(a) shows the adsorption capacity for RhB in different adsorbed times. As can be seen, the adsorption capacities of RhB were 4.58, 3.50, and 3.38 mg g^{-1} for the composite nanorods with MoO_3:S=1:0.25, MoO_3:S=1:2, and MoO_3:S=1:3, respectively.

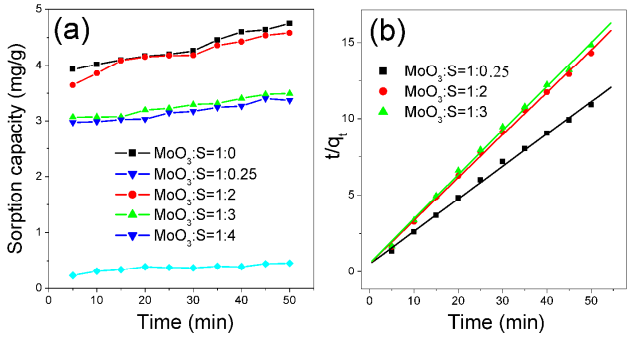

Figure 6. (a) Adsorption curves of RhB by MoO_3, MoO_2/Mo_4O_{11}, MoO_2/MoS_2, and MoS_2 composite nanorods versus contact time in water. (b) The pseudo-second order sorption kinetics of RhB onto MoO_2/Mo_4O_{11} and MoO_2/MoS_2 composite nanorods.

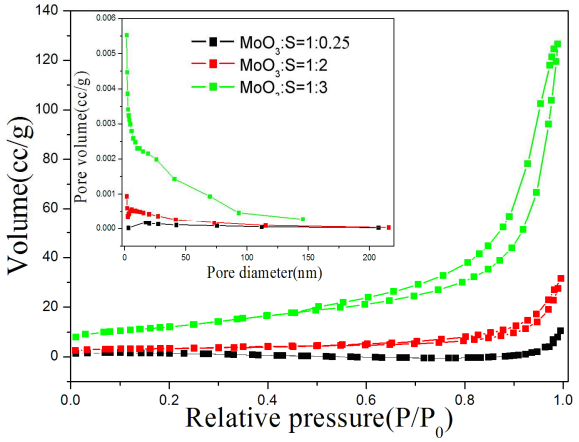

Figure 7. N_2 adsorption-desorption isotherm curves and pore size distribution (inset) of MoO_2/Mo_4O_{11} and MoO_2/MoS_2 composite nanorods with different MoO_3:S mass ratios..

Table 2. Kinetic parameters for adsorption of RhB on the samples.

Samples	q_e(exp.) (mg g^{-1})	Pseudo-first-order q_e(cal.) (mg g^{-1})	Pseudo-first-order k_1(min^{-1})	Pseudo-second-order q_e(cal.) (mg g^{-1})	Pseudo-second-order k_2(g mg^{-1} min^{-1})	R^2
MoO_3:S=1:0.25	4.58	1.4926	0.0616	4.6183	0.1318	0.997
MoO_3:S=1:2	3.50	1.0157	0.0679	3.5170	0.2119	0.999
MoO_3:S=1:3	3.38	0.5928	0.0404	3.4066	0.2201	0.998

It is well known that the adsorption performance was closely related to the ratio surface areas of samples. N_2 adsorption-desorption isotherms and the corresponding BJH pore size distribution plots of the as-obtained composite nanorods with different MoO_3:S mass ratios were performed to determine the surface area of the samples, as shown in Figure 7. The BET surface areas are 4.6455 m^2/g, 11.5271 m^2/g, and 42.4063 m^2/g

for the composite nanorods with MoO_3:S=1:0.25, MoO_3:S=1:2, and MoO_3:S=1:3, respectively. Of course, the adsorption performance should be also related to the ionic radius of metal ions.

To investigate the mechanism of adsorption, kinetic models such as pseudo-first-order and pseudo-second-order have been exploited to analyze the experimental data and applied for the adsorption of the dye on the adsorbents. The slope and the intercept of each linear plot in Figure S1 in ESI and Figure 6(b) are used to calculate the adsorption rate constants (k_1 and k_2) and the amount of adsorption in equilibrium (q_e). The calculated kinetics parameters for adsorption of the dye onto the composite nanorods are listed in Table 2. It was found that the calculated q_e (cal.) values from the pseudo-second-order kinetic equation agree well with experimental q_e (exp.). Thus, the experiment results imply that the rate limiting steps in adsorption of dye are chemical sorption involving valence forces through the sharing or exchange of electrons between adsorbent and dye.[15]

For comparison, the performance of MoO_3 and MoS_2 was also evaluated by the adsorption performance of RhB in aqueous solution, as shown in Figure 6(a). In comparison with MoO_2/Mo_4O_{11} and MoO_2/MoS_2 composite nanorods, the MoO_3 can present higher adsorption performance, however, the MoS_2 present lower adsorption performance. The adsorption capacities of RhB were 4.75 mg g^{-1} for the MoO_3 nanorods. Figure S2 shows the N_2 adsorption-desorption isotherms and the corresponding BJH pore size distribution plots of the MoO_3 nanorods. The BET surface area is 2.3306 m^2/g for the MoO_3 nanorods.

Figure S3(a) in ESI shows the adsorption capacity for Cu^{2+} ions of MoO_2/Mo_4O_{11} in different adsorbed times. The kinetics parameters for metal ions were analyzed using the pseudo-first and second kinetic equations and the linear plots were shown in Figure S3(b) and Figure S4 in ESI. The calculated q_e values agreed very well with the experimental data, suggesting that the adsorption of Cu^{2+} ions on the adsorbent also follows the pseudo-second-order kinetic model. In addition, the adsorption capacities for Zn^{2+}, Cr^{3+}, and Pb^{2+} ions by MoO_2/Mo_4O_{11} in aqueous solution are shown in Figure S5.

4. Conclusions

In summary, pure orthorhombic phase MoO_3 nanorods were synthesized by a hydrothermal method first, and then MoO_2/Mo_4O_{11} and MoO_2/MoS_2 composite nanorods were obtained by reducing MoO_3 nanorods. The adsorption performance of samples was evaluated by using RhB and Cu^{2+} ions in aqueous solutions as the target. The results indicated that the obtained MoO_2/Mo_4O_{11} and MoO_2/MoS_2 composite nanorods can present high adsorption performance. The BET surface areas are 4.6455 m^2/g, 11.5271 m^2/g, and 42.4063 m^2/g for the composite nanorods with MoO_3:S=1:0.25, MoO_3:S=1:2, and MoO_3:S=1:3, respectively. The adsorption kinetics for the Cu^{2+} ions as well as RhB on the composite nanorods were well fitted to a pseudo-second order model.

Acknowledgments

This work was supported by the National Natural Science Foundation of China (21171052, 21471050, 21473051, and 51372071), the Program for New Century Excellent Talents in University of Ministry of Education of China (NCET-11-0959), Heilongjiang Province Natural Science Foundation of Key Projects (ZD201301), Heilongjiang University Excellent Youth Foundation (JCL201102), and Harbin Technological Innovation Talent of Special Funds (RC2013QN017028).

References

1 X. Wang, J. Zhuang, Q. Peng, Y. Li, *Nature* **2005**, *437*, 121.
2 G. Wang, Q. Peng, Y. Li, *J. Am. Chem. Soc*. **2009**, *131*, 14200.
3 G. Wang, Y. Li, B. Jiang, K. Pang, N. Fan, Q. Feng, Y. Chen, C. Tian, *Chem. Commun.* **2011**, *47*, 8019.
4 J. Hui, X. Wang, *Inorg. Chem. Front.* **2014**, *1*, 215.
5 J. Hui, Q. Yu, Y. Long, Z. Zhang, Y. Yang, P. Wang, B. Xu, X. Wang, *Chem. Eur. J.* **2012**, *18*, 13702.
6 N. Liu, W. Qin, G. Qin, T. Jiang, D. Zhao, *Chem. Commun*. **2011**, *47*, 7671.
7 Z. Hou, C. Li, P. Ma, Z. Cheng, X. Li, X. Zhang, Y. Dai, D. Yang, H. Lian, J. Lin, *Adv. Funct. Mater*. **2012**, *22*, 2713.
8 F. Wang, X. Liu, *J. Am. Chem. Soc.* **2008**, *130*, 5642.
9 Y. Dai, H. Xiao, J. Liu, Q. Yuan, P. Ma, D. Yang, C. Li, Z. Cheng, Z. Hou, P. Yang, J. Lin, *J. Am. Chem. Soc.* **2013**, *135*, 18920.
10 Z. Xia, J. Zhuang, L. Liao, *Inorg. Chem.* **2012**, *51*, 7202.
11 G. Wang, Q. Peng, Y. Li, *Acc. Chem. Res.* **2011**, *44*, 322.
12 J. Nriagu, J. Pacyna, *Nature* **1988**, *333*, 134.
13 Z. Wu, D. Zhao, *Chem. Commun*. **2011**, *47*, 3332.
14 D. Lewis, A. Garrison, K. Wommack, A. Whittemore, P. Steudler, J. Melillo, *Nature* **1999**, *401*, 898.
15 L. Sun, C. Tian, L. Wang, J. Zou, G. Mu, H. Fu, *J. Mater. Chem.* **2011**, *21*, 7232.
16 A. Ramesh, H. Hasegawa, W. Sugimoto, T. Maki, K. Ueda, *Bioresour. Technol*. **2008**, *99*, 3801.
17 M. Paul, N. Pal, P. Rajamohanan, B. Rana, A. Sinha, A. Bhaumik, *Phys. Chem. Chem. Phys*. **2010**, *12*, 9389.
18 Z. Hubicki, A. Wo1owicz, *Hydrometallurgy* **2009**, *96*, 159.
19 W. Ngah, M. Hanafiah, *Bioresour. Technol*. **2008**, *99*, 3935.
20 S. Wang, H. Ang, M. Tadé, *Chemosphere* **2008**, *72*, 1621.
21 S. Liu, G. Wang, Y. Li, L. Meng, *Sci. Adv. Mater*. **2014**, *6*, 361.

